ATLAS CONF Note

ATLAS-CONF-2022-024

1st April 2022

# Strong constraints on jet quenching in centrality-dependent $p$+Pb collisions at 5.02 TeV from ATLAS

The ATLAS Collaboration

Jet quenching is the process of color-charged partons losing energy via interactions with quark-gluon plasma droplets created in heavy-ion collisions. The collective expansion of such droplets is well described by viscous hydrodynamics. Similar evidence of collectivity is consistently observed in smaller collision systems, including $pp$ and $p$+Pb collisions. In contrast, while jet quenching is observed in Pb+Pb collisions, no evidence has been found in these small systems to date, raising fundamental questions about the nature of the system created in these collisions. The ATLAS experiment at the Large Hadron Collider measured the yield of charged hadrons correlated with reconstructed jets in 0.36 nb$^{-1}$ of $p$+Pb and 3.6 pb$^{-1}$ of $pp$ collisions at 5.02 TeV. The yields of hadrons with $p_{\mathrm{T}}^{\mathrm{ch}} > 0.5$ GeV near and opposite in azimuth to jets with $p_{\mathrm{T}}^{\mathrm{jet}} > 30, 60$ GeV, and the ratios of these yields between $p$+Pb and $pp$ collisions, $I_{p\mathrm{Pb}}$, are reported. The collision centrality of $p$+Pb events is categorized by the energy deposited by forward neutrons from the struck nucleus. The $I_{p\mathrm{Pb}}$ values are consistent with unity within a few percent for hadrons with $p_{\mathrm{T}}^{\mathrm{ch}} > 4$ GeV at all centralities. These data provide new, strong constraints which preclude almost any parton energy loss in central $p$+Pb collisions.

ATLAS-CONF-2022-024
11 April 2022

Over two decades of measurements of relativistic nucleus–nucleus collisions at the Relativistic Heavy Ion Collider (RHIC) and the Large Hadron Collider (LHC) have established that a quark-gluon plasma is formed in these collisions which undergoes a collective expansion described by viscous hydrodynamics [1]. High-momentum colored probes, such as quarks and gluons, lose significant energy as they traverse the plasma and produce a highly modified hadron fragmentation pattern, a process referred to as "jet quenching" [2–4]. On the other hand, colorless photons and $Z$-bosons pass through unscathed [5–9]. Over the past decade, measurements in smaller collisions systems, such as $pp$ and $p$+Pb at the LHC and $p$+Au, $d$+Au, and $^3$He+Au at RHIC, revealed a similar collective motion which can also be described via viscous hydrodynamics [10, 11]. These observations have prompted significant theoretical discussion as to whether jet quenching should be present in these small systems as well [12–18]. However, measurements of jet [19, 20] and hadron [21–23] production rates at high transverse momentum ($p_{\mathrm{T}}$) [1] and measurements of jet-to-hadron fragmentation functions [24] in minimum-bias $p$+Pb collisions show no indication of jet quenching relative to $pp$ in these small systems [25].

Experiments have also examined the subset of $p$+Pb collisions where the proton undergoes many interactions in the Pb nucleus (i.e., large number of proton–nucleon collisions $\langle N_{\mathrm{coll}} \rangle$) and which typically have larger than average particle multiplicities. These so-called "central" events may produce a larger and longer-lived quark-gluon plasma which would induce a bigger jet quenching effect. Measurements which characterize the centrality of events based on the charged-particle multiplicity or energy at mid-rapidity have found significant deviations of high-$p_{\mathrm{T}}$ charged-hadron production rates from the $pp$ expectation [26]. However, Monte Carlo (MC) simulations using the HIJING [27] generator, and other models of small collision systems, indicate that the large majority of this behavior is the result of physics correlations between the charged-particle multiplicity and the probability to produce a high-$p_{\mathrm{T}}$ jet or hadron in individual proton–nucleon collisions [26, 28]. In addition, in extreme kinematic regions such as those with large Bjorken-$x$, the production of high-$p_{\mathrm{T}}$ jets or hadrons becomes anti-correlated with the centrality signal [19, 29] which may arise from, for example, the decreasing interaction strength of protons in these configurations [30, 31] or other effects [32, 33]. Model-dependent corrections for the effect of these correlations can be derived [34, 35], but they have strongly limited the precision of searches for jet quenching phenomena in central $p$+Pb events.

An alternative method, which does not exhibit the physics biases above, is to select central $p$+Pb events by counting the number of spectator neutrons produced by the disintegrating Pb nucleus in a Zero Degree Calorimeter (ZDC), where more spectator neutrons correlates with more central events. However, estimating the $\langle N_{\mathrm{coll}} \rangle$ in the resulting event categories is challenging due to the limited understanding of how spectator nucleons are distributed in terms of single neutrons, protons, and larger charged fragments (only the first of which strike the ZDC). Nevertheless, the ALICE experiment has used this method to find that rates of charged [26] and heavy-flavor [36] hadrons in central $p$+Pb collisions are unmodified when compared to those derived from $pp$ interactions, albeit within significant modeling uncertainties. To avoid the reliance on $\langle N_{\mathrm{coll}} \rangle$, jet quenching in these events may instead be searched for by examining the internal structure of jets or jet–hadron kinematic correlations. A measurement of hadron–triggered jet yields in ZDC-selected central $p$+Pb events has placed limits on the total amount of energy transported across the boundary of an $R = 0.4$ jet cone [37], which is one possible signature. However, to further enhance the sensitivity to jet quenching effects

[1] ATLAS uses a right-handed coordinate system with its origin at the nominal interaction point (IP) in the center of the detector and the $z$-axis along the beam pipe. The x-axis points from the IP to the centre of the LHC ring, and the y-axis points upward. Cylindrical coordinates $(r, \phi)$ are used in the transverse plane, $\phi$ being the azimuthal angle around the $z$-axis. The pseudorapidity is defined in terms of the polar angle $\theta$ as $\eta = -\ln\tan(\theta/2)$.

in small collision systems and maximally constrain any possible signal, a study sensitive to the internal jet hadron structure in spectator–neutron–selected central $p$+Pb collisions is required.

This note presents a measurement of the yield of charged hadrons produced in events containing calorimeter jets with two different selections ($p_{\mathrm{T}}^{\mathrm{jet}} > 60$ GeV or $p_{\mathrm{T}}^{\mathrm{jet}} > 30$ GeV) in $p$+Pb and $pp$ collisions at a nucleon–nucleon center-of-mass energy 5.02 TeV, recorded with the ATLAS detector. The $p$+Pb and $pp$ data were recorded in 2016 and 2017, respectively, with triggers that have integrated luminosities of $0.36\,\mathrm{nb}^{-1}$ and $3.6\,\mathrm{pb}^{-1}$. In $p$+Pb running, the proton and Pb beams have energies of 4 TeV and $(Z/A) \times 4$ TeV$\approx 1.58$ TeV, respectively, leading to a rapidity shift of the center-of-mass frame, $\Delta y^{\mathrm{com}} = 0.465$, from the laboratory frame (while $y^{\mathrm{com}} = 0$ in $pp$ running). Charged hadrons are required to have $p_{\mathrm{T}}^{\mathrm{ch}} > 0.5$ GeV and their yields are measured in two azimuthal regions with respect to the jet: the "away-side" region $\Delta\phi_{\mathrm{ch,jet}} = |\phi_{\mathrm{ch}} - \phi_{\mathrm{jet}}| > 7\pi/8$ and the "near-side" region $\Delta\phi_{\mathrm{ch,jet}} < \pi/8$. The total yield in each region, $Y(p_{\mathrm{T}}^{\mathrm{ch}})$, is normalized per jet and reported in $pp$ events and in $p$+Pb events under different ZDC energy selections. To quantify any modification which would result from the partons' propagation through a created quark–gluon plasma, the ratio of the per-jet charged-particle yields between $p$+Pb and $pp$ collisions, $I_{p\mathrm{Pb}} = Y_{p\mathrm{Pb}}/Y_{pp}$, is reported and compared with the expectations from theoretical calculations. Importantly, this observable does not depend on a quantitative estimate of $\langle N_{\mathrm{coll}} \rangle$.

The ATLAS experiment [38] is a multipurpose particle detector with a forward–backward symmetric cylindrical geometry and a near $4\pi$ coverage in solid angle. It consists of an inner tracking detector surrounded by a superconducting solenoid providing a 2 T axial magnetic field, electromagnetic and hadron calorimeters, and a muon spectrometer. The inner tracking detector covers the pseudorapidity range $|\eta| < 2.5$. It consists of silicon pixel, silicon microstrip, and transition radiation tracking detectors [39, 40]. Lead/liquid-argon sampling calorimeters provide electromagnetic (EM) energy measurements with high granularity. A steel/scintillator-tile hadron calorimeter covers the central pseudorapidity range ($|\eta| < 1.7$). Liquid-argon calorimeters with separate EM and hadronic compartments instrument the endcap (up to $|\eta| = 3.2$) and forward (FCal, up to $|\eta| = 4.9$) regions. Two ZDCs are each composed of four longitudinal layers of tungsten absorbers and quartz rods. They are situated in the far forward region $|\eta| > 8.3$ and, in $p$+Pb events, the ZDC downstream of the Pb beam direction measures primarily spectator neutrons from the struck Pb nucleus. An extensive software suite [41] is used in the reconstruction and analysis of real and simulated data, in detector operations, and in the trigger and data acquisition systems of the experiment.

Events are selected for analysis using a combination of minimum-bias and calorimeter jet triggers [42], which are used for the measurements with $p_{\mathrm{T}}^{\mathrm{jet}} > 30$ GeV and $> 60$ GeV, respectively. Both $pp$ and $p$+Pb events are required to have a primary reconstructed vertex with $z$ coordinate $|z| < 150$ mm [43]. The $pp$ and $p$+Pb data are from low collision rate data taking, and an additional requirement that events have only one reconstructed interaction vertex further reduces pileup. In the $pp$ ($p$+Pb) data this requirement accepts approximately 40% (99%) of triggered events.

The centrality of $p$+Pb events is characterized using the total energy in the Pb-going side of the ZDC, i.e., the ZDC on the side corresponding to the direction of the Pb beam. The ZDC energy is calibrated by matching the single and double neutron peaks to their known beam energies (1.58 TeV and 3.15 TeV), and the resulting energy distribution is shown in Figure 1. As described above, this results in an unbiased event selection with which to search for jet quenching. Using a ZDC with similar acceptance, the ALICE Collaboration has used multiple bootstrapping methods to estimate that the $\langle N_{\mathrm{coll}} \rangle$ values in these events range from approximately

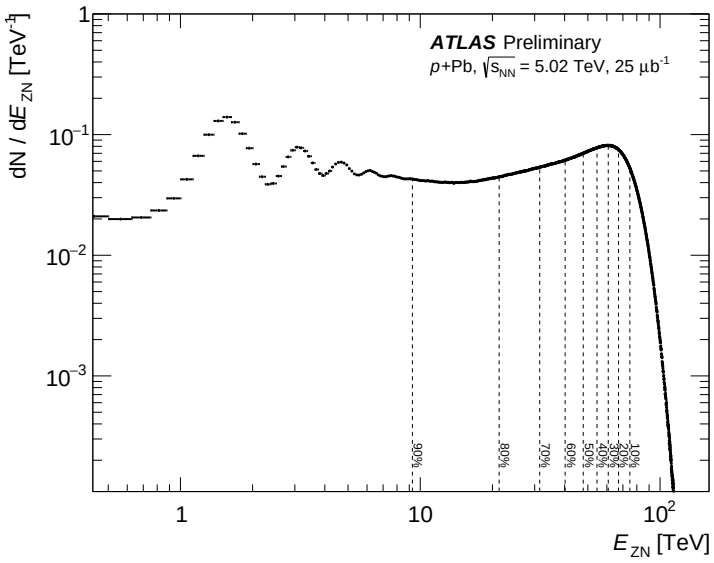


Figure 1: Distribution of energy measured in the Pb-going side of the Zero Degree Calorimeter ($E_{\mathrm{ZN}}$) in $p$+Pb collisions at 5.02 TeV selected with a minimum-bias trigger. Dashed vertical lines indicate the boundaries between 0-10%, 10-20%, etc. centrality selections.

13.6 (±11%) in 0–20% $p$+Pb events to 1.2 (±24%) in 80–100% events [26]. These values and uncertainties are not explicitly used in the measurement in this note but may be useful for modeling comparisons.

Jets are reconstructed from calorimeter deposits using the anti-$k_T$ algorithm [44, 45] with cone size $R = 0.4$ using the procedure described in Ref. [46]. The jet kinematics are corrected event-by-event for the contribution from underlying event (UE) particles, and are calibrated using simulations [41] of the calorimeter response and *in situ* measurements of the absolute energy scale in data. They are required to lie within $|\eta| < 2.8$.

Reconstructed charged-particle tracks are required to have $p_{\mathrm{T}}^{\mathrm{ch}} > 0.5$ GeV, lie within $|\eta - y^{\mathrm{com}}| < 2.035$, and satisfy quality criteria outlined in Ref. [47]. The charged-particle yield is corrected for the finite reconstruction and selection efficiency with a per-track weight, and for the small contribution from secondary-particle and fake tracks, with both corrections derived from Monte Carlo Pythia8 [48] $pp$ and Hijing [27] $p$+Pb samples. The contribution of UE particles to the total yields is estimated by measuring these yields in minimum-bias $p$+Pb or $pp$ events with the same selection requirements and with matched intervals in FCal energy (which is well-correlated with UE activity [49]). The UE contribution is subtracted from the yield measured in jet-containing events. The signal to UE background ratio is approximately 0.25 for $p_{\mathrm{T}}^{\mathrm{ch}} < 1$ GeV in central events, with the UE contribution quickly becoming negligible at higher $p_{\mathrm{T}}^{\mathrm{ch}}$ or in less central events. Finally, the finite resolution in the $p_{\mathrm{T}}^{\mathrm{jet}}$ and $p_{\mathrm{T}}^{\mathrm{ch}}$ values results in a distortion of the measured yields. This effect is typically smaller than 10% and is similar in $p$+Pb and $pp$. It is corrected for via an iterative Bayesian unfolding procedure [50] applied to the two-dimensional $(p_{\mathrm{T}}^{\mathrm{jet}}, p_{\mathrm{T}}^{\mathrm{ch}})$ distributions derived from Monte Carlo Pythia8 $pp$ and Pythia8 with $p$+Pb data overlay samples.

The dominant sources of systematic uncertainty in the measurement are those affecting the measurement of the jet kinematics, the charged-particle selection, and the unfolding correction. The jet-related uncertainties are

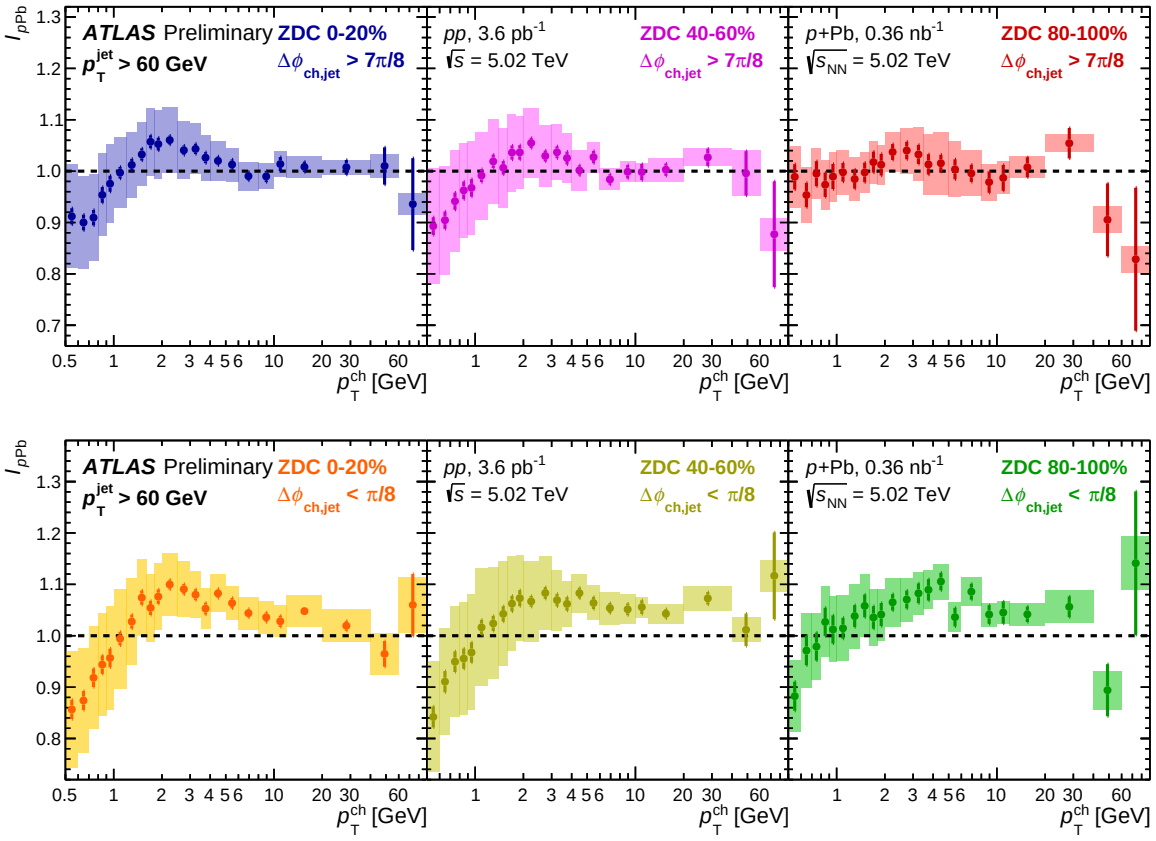


Figure 2: The ratio of per-jet charged particle yields between $p$+Pb and $pp$ collisions, $I_{p\mathrm{Pb}}$, for hadrons opposite ($\Delta\phi_{\mathrm{ch,jet}} > 7\pi/8$; top row) and near ($\Delta\phi_{\mathrm{ch,jet}} < \pi/8$; bottom row) a $p_{\mathrm{T}}^{\mathrm{jet}} > 60$ GeV jet . Results are shown for different ZDC-selected $p$+Pb centralities in each column. Statistical uncertainties are shown as vertical lines and systematic uncertainties as filled boxes.

derived from *in situ* studies of the calorimeter response [51] and their application to the jets used in heavy-ion data [52], and from the comparison of the simulated response in different generators. They typically dominate at high-$p_{\mathrm{T}}^{\mathrm{ch}}$. Several sources of tracking-related uncertainty are considered, such as the uncertainty in the absolute efficiency and the sensitivity to selection cuts. They are described in previous measurements of charged-particle fragmentation functions [24, 53] and typically dominate at low-$p_{\mathrm{T}}^{\mathrm{ch}}$. The uncertainty in the unfolding correction is evaluated by considering different priors and by performing the analysis procedure, including the UE subtraction, in simulation to evaluate how accurately the generator-level distributions are recovered. This uncertainty is significant at all $p_{\mathrm{T}}^{\mathrm{ch}}$. Many of these uncertainties, such as the jet-related ones, have a quantitatively similar impact on the yields in the $p$+Pb and $pp$ data and cancel to a significant degree in the $I_{p\mathrm{Pb}}$ ratio.

Figure 2 (top row) shows the $I_{p\mathrm{Pb}} = Y_{p\mathrm{Pb}}/Y_{pp}$ ratios for charged particles on the away-side of jets with $p_{\mathrm{T}}^{\mathrm{jet}}$ > 60 GeV. In the region $p_{\mathrm{T}}^{\mathrm{ch}} > 1$ GeV, the $I_{p\mathrm{Pb}}$ values in all centrality selections are consistent with unity within the uncertainties. At the lowest measured $p_{\mathrm{T}}^{\mathrm{ch}}$ values, the $I_{p\mathrm{Pb}}$ decreases to about 10% below unity,

albeit with growing uncertainties. In a leading-order parton–parton scattering picture, the away-side hadrons arise from the fragmentation of $p_{\mathrm{T}} \approx 60$ GeV partons azimuthally opposite to the parton producing the jet. A jet quenching effect in $p$+Pb should lead to $I_{p\mathrm{Pb}}$ values below unity. As such, these results set a strong constraint on any possible modification of parton fragmentation in the region $z = p_{\mathrm{T}}^{\mathrm{ch}}/p_{\mathrm{T}}^{\mathrm{jet}} \approx 0.05$–$1.0$, within uncertainties that decrease to 2–4% at high-$z$. Since $pp$ collisions also have indicators of collective flow [54], it should not be automatically ruled out that quenching effects are present in both $pp$ and central $p$+Pb at very similar levels.

Figure 2 (bottom row) shows the $I_{p\mathrm{Pb}}$ ratios for charged particles on the near-side of jets with $p_{\mathrm{T}}^{\mathrm{jet}} > 60$ GeV. In the region $p_{\mathrm{T}}^{\mathrm{ch}} > 4$ GeV, there is a centrality-independent enhancement of approximately 5%. Similar to that observed on the away side, there is a characteristic suppression in the region $p_{\mathrm{T}}^{\mathrm{ch}} < 1$ GeV. Additionally, the $I_{p\mathrm{Pb}}$ shows a modest systematic enhancement in the region $1 < p_{\mathrm{T}}^{\mathrm{ch}} < 4$ GeV. It is notable that the pattern from $0.5 - 4$ GeV is consistent between the away- and near-side, and also with the inclusive charged-hadron $R_{p\mathrm{Pb}}$ [55], where the $R_{p\mathrm{Pb}}$ is often interpreted in terms of initial-state parton scattering in the nuclear target, also known as the "Cronin" effect [56]. In heavy-ion collisions, the "soft" particle production regime is describable via hydrodynamics and it is known that the radial flow of the quark–gluon plasma may play a role in this $p_{\mathrm{T}}^{\mathrm{ch}}$ region. The measurement in this note suggests that low-$p_{\mathrm{T}}$ particles which arise from jet fragmentation also exhibit a similar pattern.

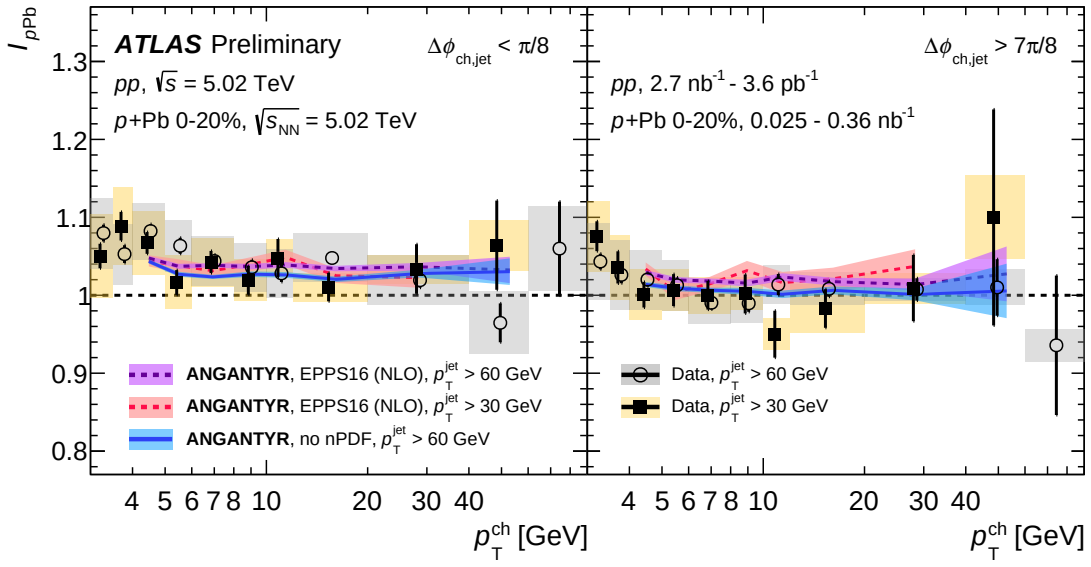


Figure 3: The ratio of per-jet charged particle yields $I_{p\mathrm{Pb}}$ on the near-side (left) and away-side (right) between $p$+Pb and $pp$ are plotted for the 0-20% $p$+Pb ZDC-selected centralities. Particles correlated with a jet above 30 GeV and 60 GeV are shown. Statistical uncertainties are shown as vertical lines and systematic uncertainties as filled boxes. Also shown are calculations from the ANGANTYR generator [57] with (EPPS16 (NLO)) and without (no PDF) nuclear-modified parton distribution functions [58]. ANGANTYR results are only shown for $p_{\mathrm{T}}^{\mathrm{ch}} > 4.5$ GeV where no UE subtraction is necessary. The colored bands represent statistical uncertainties only.

The same measurements were also performed for jets with $p_{\mathrm{T}}^{\mathrm{jet}} > 30$ GeV, which are sensitive to quenching effects on lower-$p_{\mathrm{T}}$ partons. These are shown in Figure 3, focusing on $p_{\mathrm{T}}^{\mathrm{ch}} > 4$ GeV and 0–20% ZDC-selected

events to emphasize the region of potential jet quenching. Within the larger uncertainties, which arise from the larger relative UE background, poorer jet energy resolution, and smaller sampled luminosity, they are compatible with the $p_{\mathrm{T}}^{\mathrm{jet}} > 60$ GeV results. Since the near-side $I_{p\mathrm{Pb}}$ is similar to a modified jet fragmentation function, it can be compared with the previous measurement in $p$+Pb collisions by ATLAS [24]. For jets in a similar $p_{\mathrm{T}}^{\mathrm{jet}}$ range, the ratios of fragmentation functions in $p$+Pb to $pp$ collisions in Ref. [24] are compatible with the results in this note, although with larger uncertainties due to the different datasets used.

In Figure 3, the $I_{p\mathrm{Pb}}$ measurements are also compared to calculations from the heavy-ion MC generator Angantyr [57] run in $p$+Pb mode. Angantyr is based on Pythia8 [48] and has no final-state effects producing collectivity or jet quenching - noting that this is run with so-called "string shoving" turned off [59]. Angantyr shows similar near-side enhancement as the data, and studies with the generator settings indicate that this does not arise from either the nuclear modification of parton densities, or the different isospin composition of Pb nuclei compared to protons. On the away-side, the generator features a small enhancement, but is also compatible with the data within its uncertainties.

Despite clear signals of collective motion in $p$+Pb collisions suggesting that a quark–gluon plasma is formed [10], these data severely constrain the amount of jet quenching, which normally accompanies the collective motion observed in Pb+Pb collisions. It has been proposed that soft (low momentum) quarks and gluons are only formed on a time scale of 1 fm/c, and thus the high-$p_{\mathrm{T}}$ partons may undergo their virtuality evolution and showering unscathed and fragment in vacuum if the quark–gluon plasma is small, i.e., $R < 1$–$2$ fm [60]. A quantitative calculation incorporating this virtuality evolution is necessary to confront the $I_{p\mathrm{Pb}}$ measurements presented here.

This note reports a measurement of charged-hadron yields produced in the azimuthal direction away from and near to jets in $p$+Pb collisions, compared to those in $pp$ collisions, using data collected with the ATLAS detector at the LHC. Central $p$+Pb collisions, where the effects of a quark–gluon plasma are expected to be largest, are selected in an unbiased way by detecting forward spectator neutrons. The per-jet yields on the near-side indicate a modest, of order 5%, enhancement for $p_{\mathrm{T}}^{\mathrm{ch}} > 4$ GeV that is well described by the MC generator Angantyr. The per-jet yields on the away-side are consistent with unity for all $p_{\mathrm{T}}^{\mathrm{ch}} > 1$ GeV, with uncertainties that are particularly small for $p_{\mathrm{T}}^{\mathrm{ch}} > 4$ GeV. This data serves as a sensitive probe of jet quenching effects and places strong limits on the degree to which the propagation and fragmentation of hard-scattered partons is modified in small hadronic collisions. The results in this note heighten the challenge to the theoretical understanding of the produced quark–gluon system in $p$+Pb collisions.

# Appendix

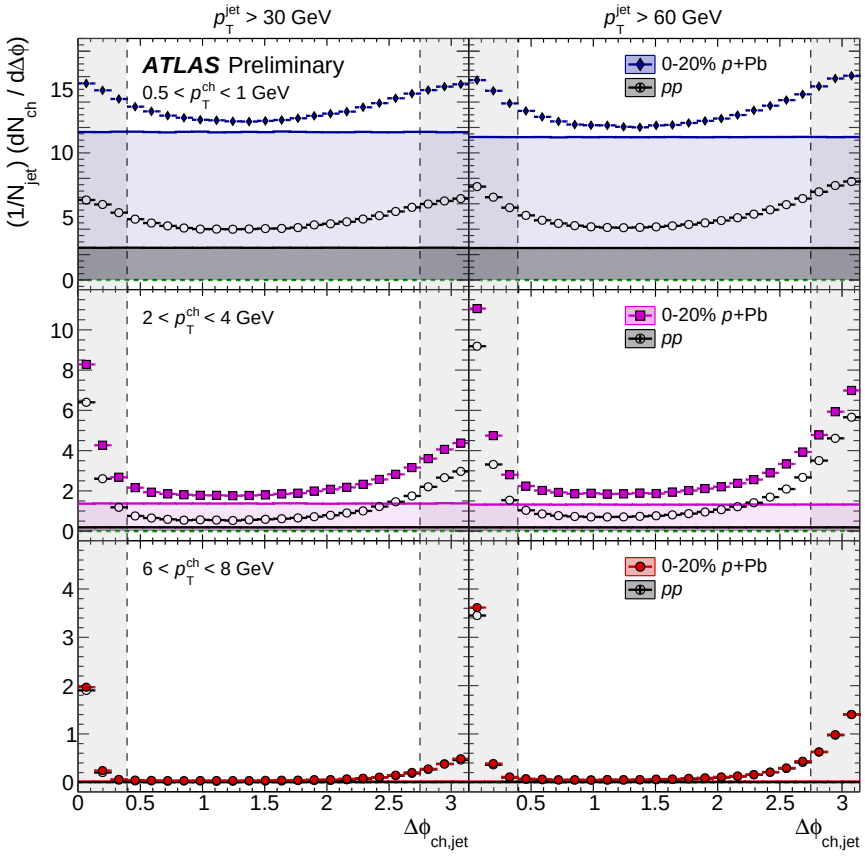


Figure 4: The per-jet charged particle yield in ZDC-selected 0–20% $p$+Pb (solid markers) and $pp$ (open markers) collisions for hadrons with low-$p_{\mathrm{T}}$ (0.5–1 GeV; top row), moderate $p_{\mathrm{T}}$ (2–4 GeV; middle row), and high $p_{\mathrm{T}}$ (6–8 GeV; bottom row), correlated to a jet with $p_{\mathrm{T}}^{\mathrm{jet}} > 30$ GeV (left column) and $p_{\mathrm{T}}^{\mathrm{jet}} > 60$ GeV (right column). The data is uncorrected for detector resolution effects. Statistical uncertainties are shown as vertical lines; no systematic uncertainties are shown. Shaded regions indicate the underlying event estimate.

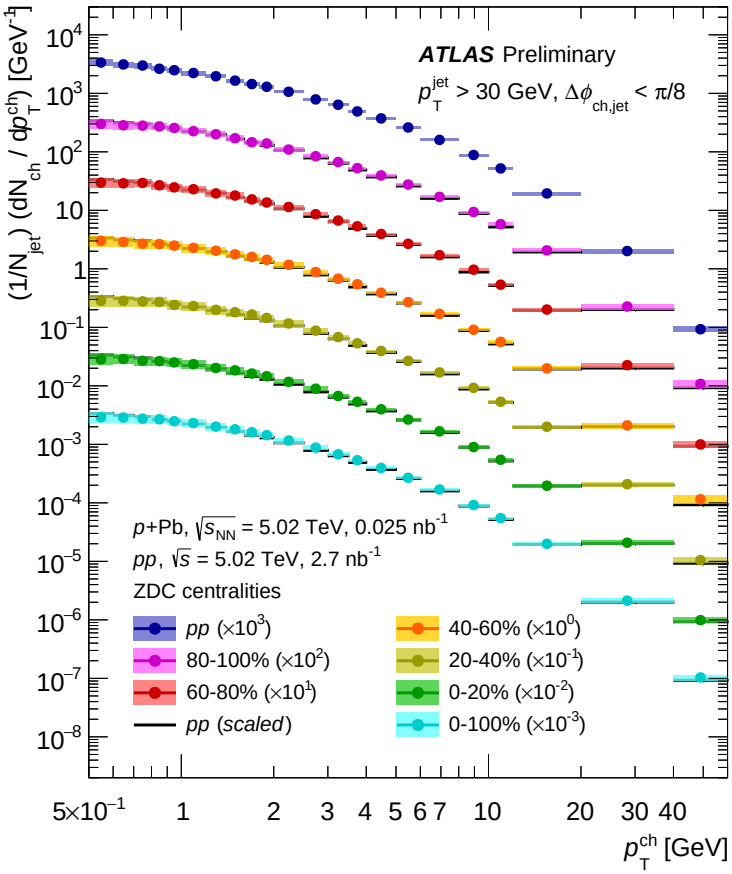


Figure 5: The per-jet charged particle yield in $p$+Pb and $pp$ collisions for hadrons near a $p_{\mathrm{T}}^{\mathrm{jet}} > 30$ GeV jet ($\Delta\phi_{\mathrm{ch,jet}} < \pi/8$). Results are shown for different ZDC-selected $p$+Pb centralities, and offset by multiples of 10 for visibility. Statistical uncertainties are shown as vertical lines and systematic uncertainties as filled boxes.

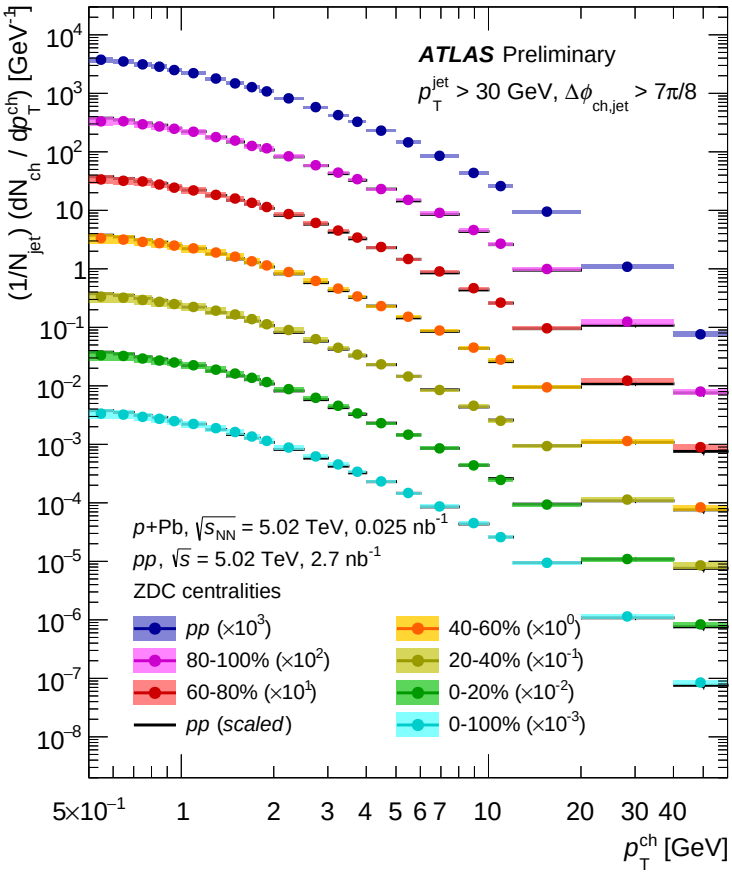


Figure 6: The per-jet charged particle yield in $p$+Pb and $pp$ collisions for hadrons opposite to a $p_{\mathrm{T}}^{\mathrm{jet}} > 30$ GeV jet ($\Delta\phi_{\mathrm{ch,jet}} > 7\pi/8$). Results are shown for different ZDC-selected $p$+Pb centralities, and offset by multiples of 10 for visibility. Statistical uncertainties are shown as vertical lines and systematic uncertainties as filled boxes.

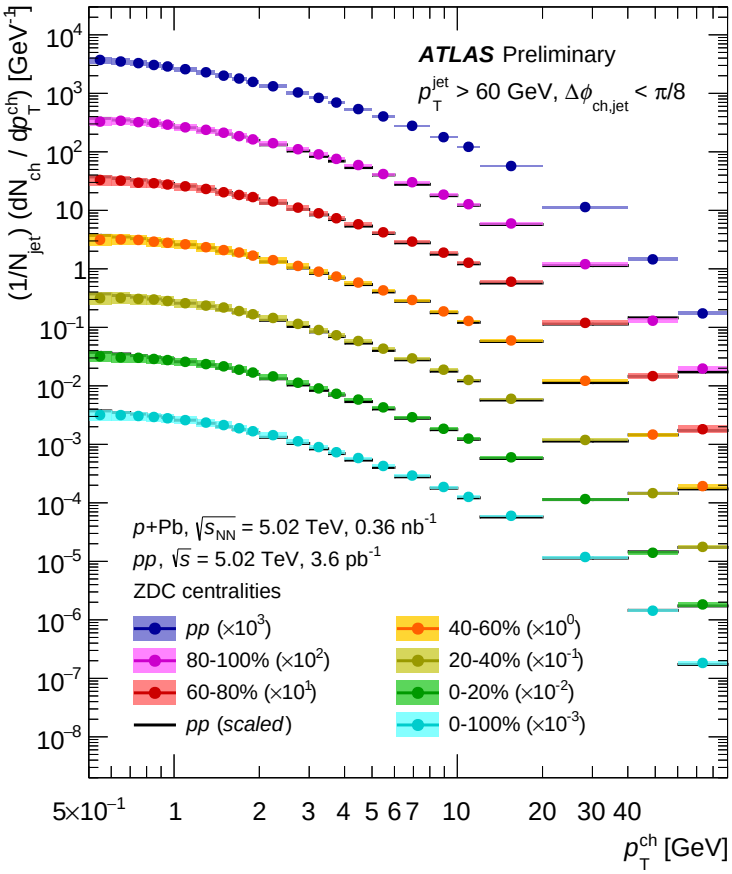


Figure 7: The per-jet charged particle yield in $p$+Pb and $pp$ collisions for hadrons near a $p_{\mathrm{T}}^{\mathrm{jet}} > 60$ GeV jet ($\Delta\phi_{\mathrm{ch,jet}} < \pi/8$). Results are shown for different ZDC-selected $p$+Pb centralities, and offset by multiples of 10 for visibility. Statistical uncertainties are shown as vertical lines and systematic uncertainties as filled boxes.

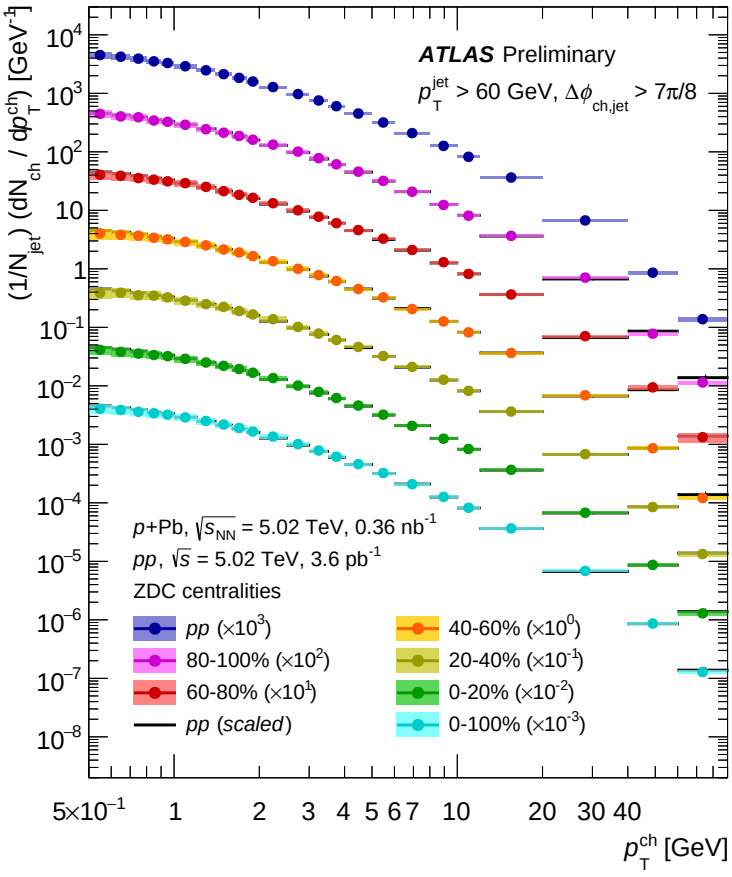


Figure 8: The per-jet charged particle yield in $p$+Pb and $pp$ collisions for hadrons opposite to a $p_{\mathrm{T}}^{\mathrm{jet}} > 60$ GeV jet ($\Delta\phi_{\mathrm{ch,jet}} > 7\pi/8$). Results are shown for different ZDC-selected $p$+Pb centralities, and offset by multiples of 10 for visibility. Statistical uncertainties are shown as vertical lines and systematic uncertainties as filled boxes.

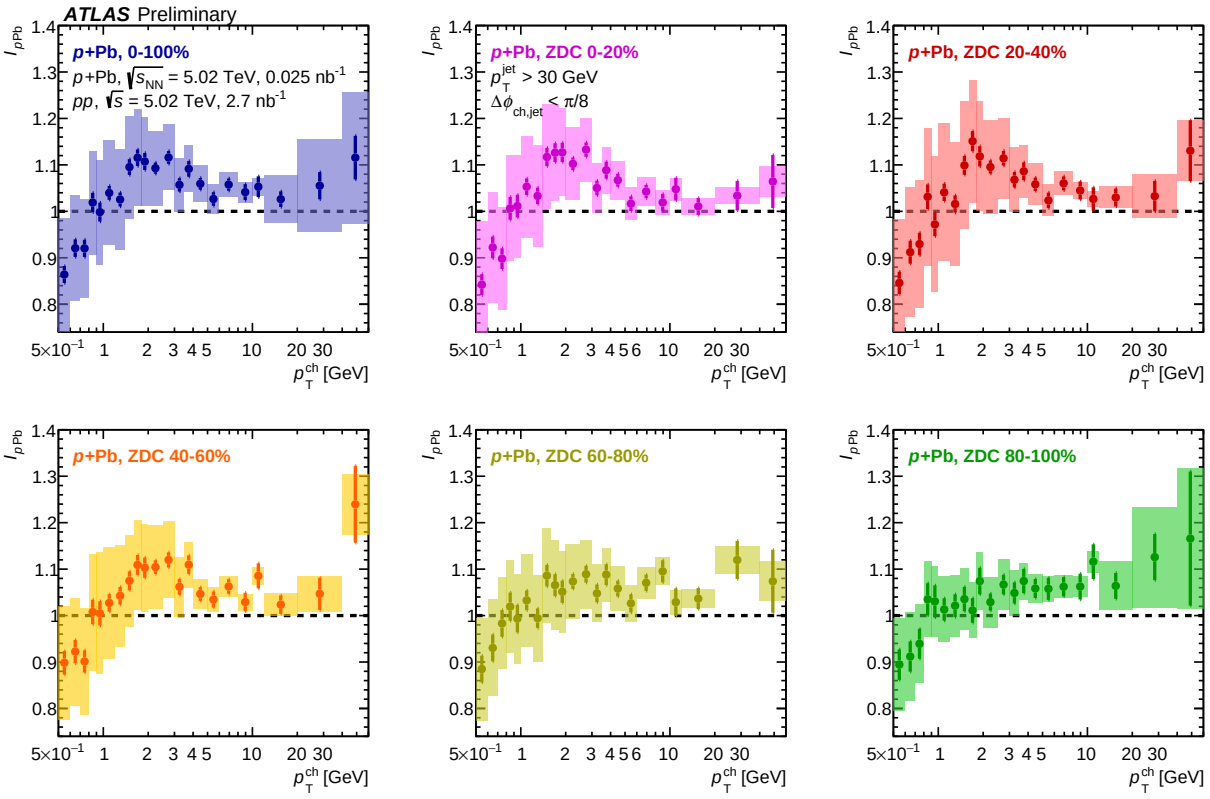


Figure 9: The ratio of per-jet charged particle yields in $p$+Pb and $pp$ collisions, $I_{p\mathrm{Pb}}$, for hadrons near a $p_{\mathrm{T}}^{\mathrm{jet}} > 30$ GeV jet ($\Delta\phi_{\mathrm{ch,jet}} < \pi/8$). Results are shown for different ZDC-selected $p$+Pb centralities in each panel. Statistical uncertainties are shown as vertical lines and systematic uncertainties as filled boxes.

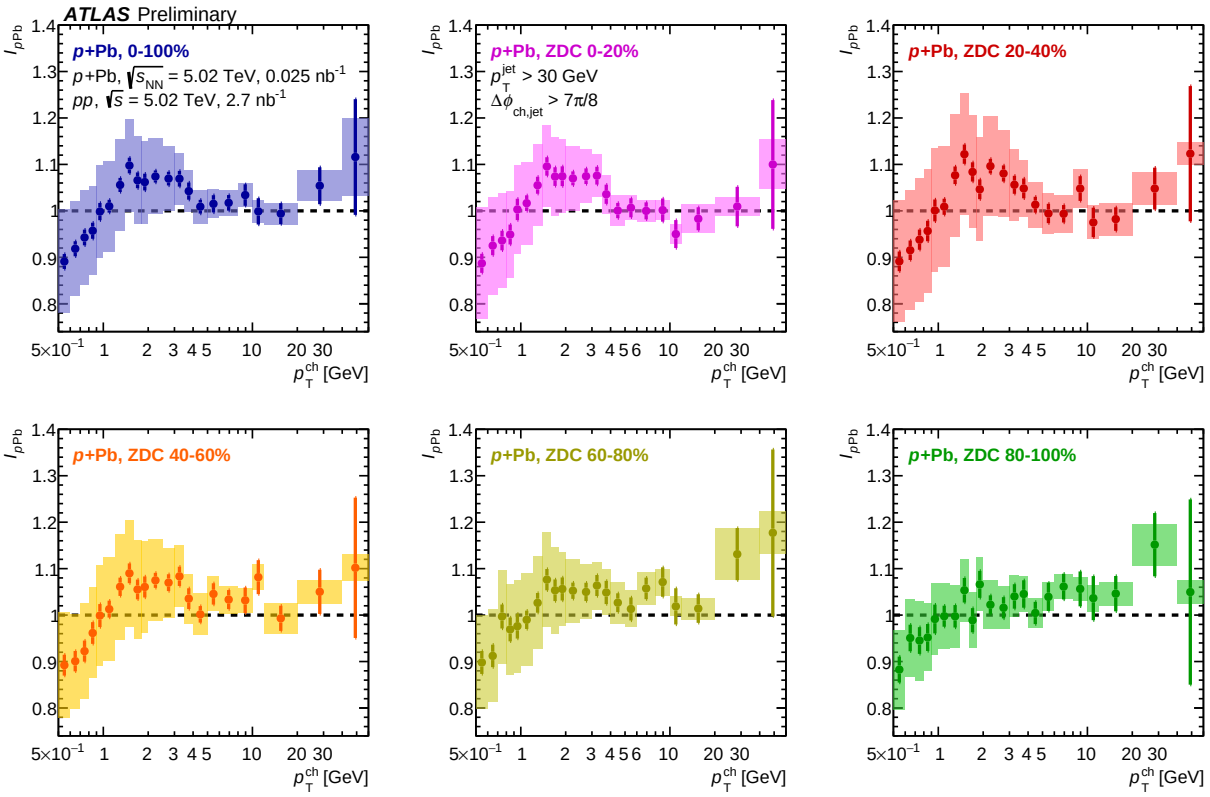


Figure 10: The ratio of per-jet charged particle yield in $p$+Pb and $pp$ collisions, $I_{p\mathrm{Pb}}$, for hadrons opposite to a $p_{\mathrm{T}}^{\mathrm{jet}} > 30$ GeV jet ($\Delta\phi_{\mathrm{ch,jet}} > 7\pi/8$). Results are shown for different ZDC-selected $p$+Pb centralities in each panel. Statistical uncertainties are shown as vertical lines and systematic uncertainties as filled boxes.

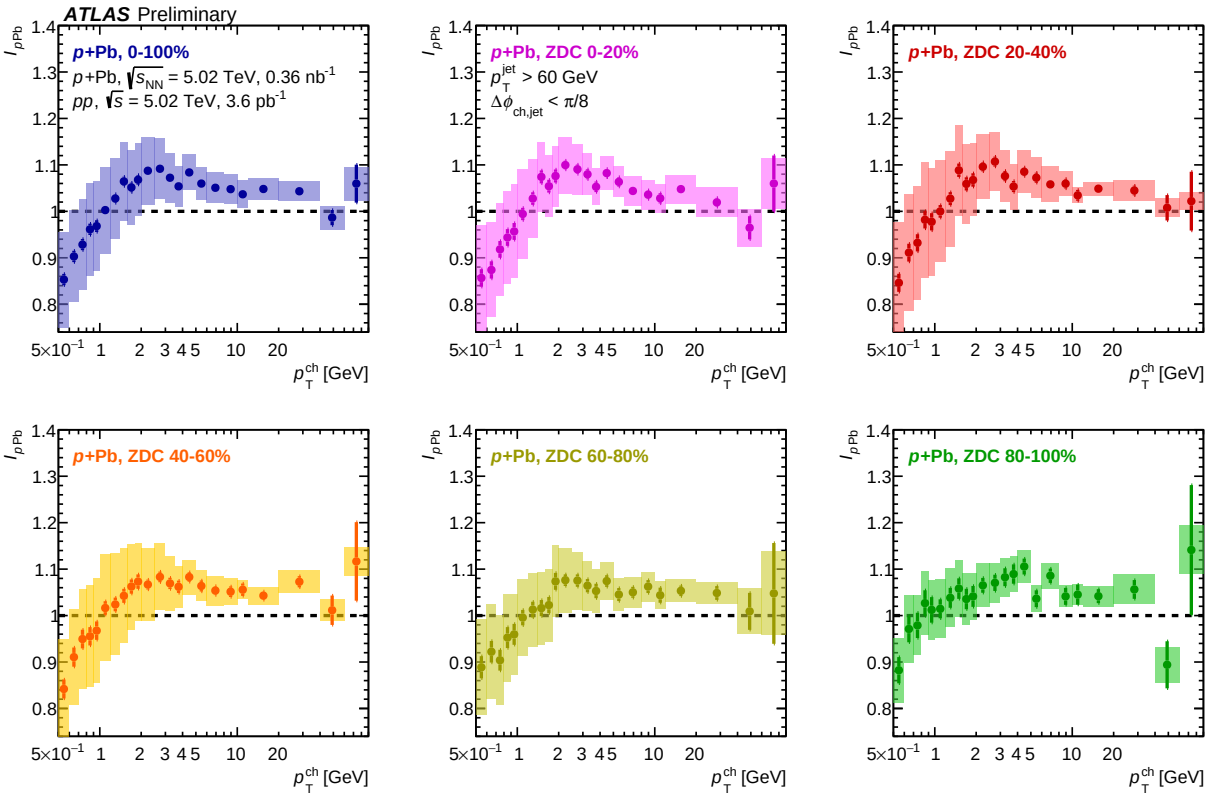


Figure 11: The ratio of per-jet charged particle yield in $p$+Pb and $pp$ collisions, $I_{p\mathrm{Pb}}$, for hadrons near a $p_{\mathrm{T}}^{\mathrm{jet}} > 60$ GeV jet ($\Delta\phi_{\mathrm{ch,jet}} < \pi/8$). Results are shown for different ZDC-selected $p$+Pb centralities in each panel. Statistical uncertainties are shown as vertical lines and systematic uncertainties as filled boxes.

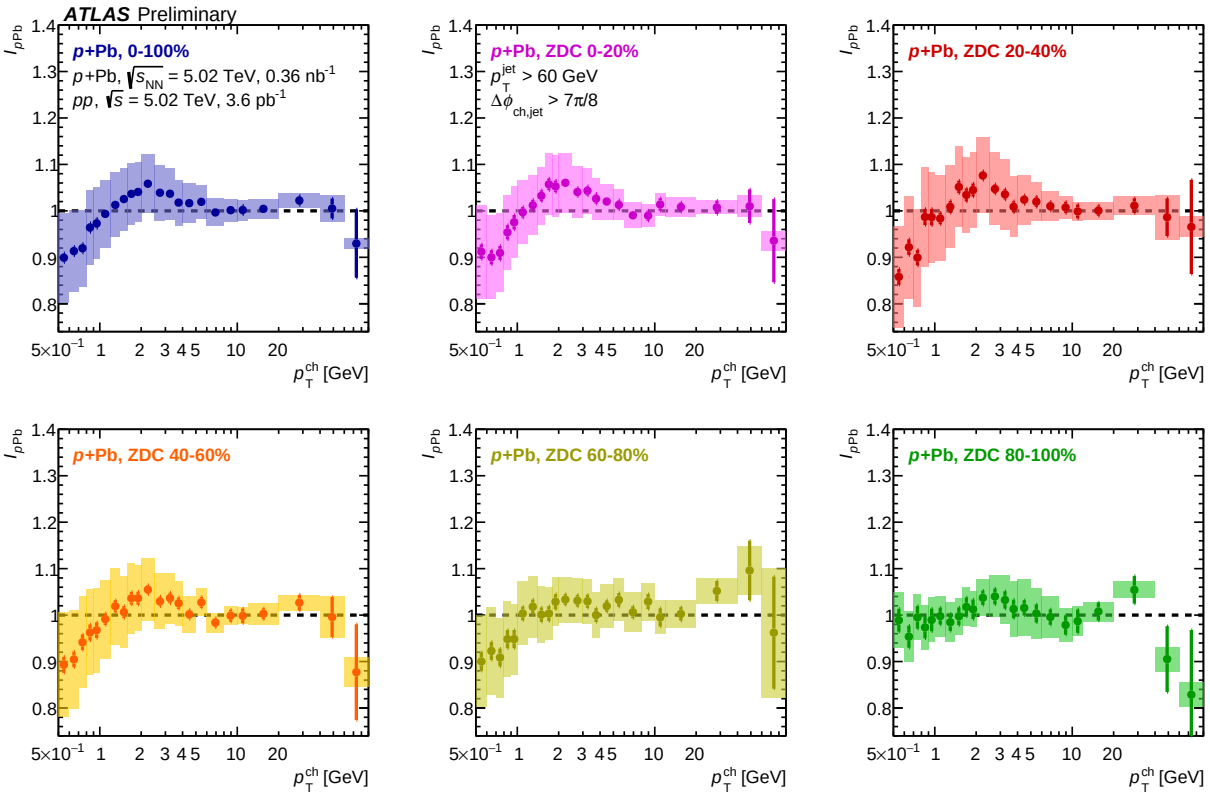


Figure 12: The ratio of per-jet charged particle yield in $p$+Pb and $pp$ collisions, $I_{p\mathrm{Pb}}$, for hadrons opposite to a $p_{\mathrm{T}}^{\mathrm{jet}} > 60$ GeV jet ($\Delta\phi_{\mathrm{ch,jet}} > 7\pi/8$). Results are shown for different ZDC-selected $p$+Pb centralities in each panel. Statistical uncertainties are shown as vertical lines and systematic uncertainties as filled boxes.

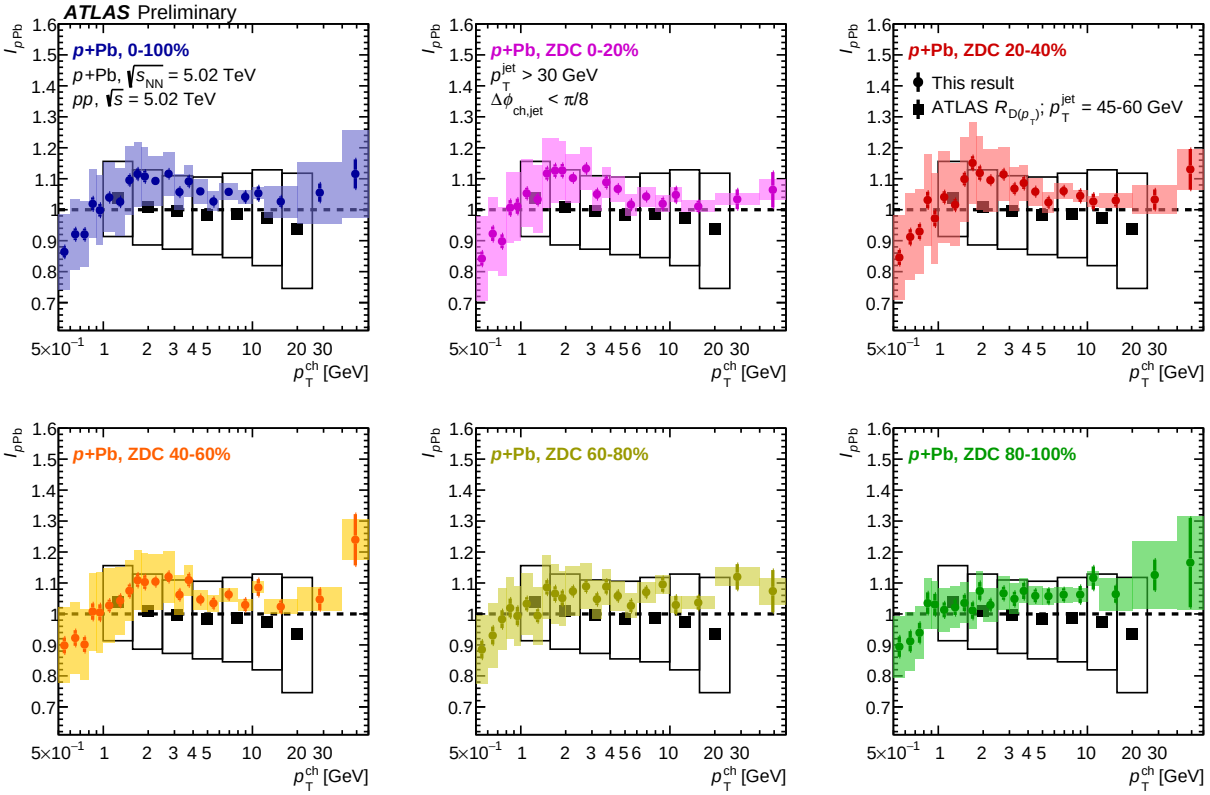


Figure 13: The ratio of per-jet charged particle yield in $p$+Pb and $pp$ collisions, $I_{p\mathrm{Pb}}$, for hadrons near a $p_{\mathrm{T}}^{\mathrm{jet}} > 30$ GeV jet ($\Delta\phi_{\mathrm{ch,jet}} < \pi/8$). Results are shown for different ZDC-selected $p$+Pb centralities in each panel. Also shown in square markers are ratios of the jet fragmentation function between centrality-inclusive $p$+Pb and $pp$ collisions for jets with $p_{\mathrm{T}}^{\mathrm{jet}} = 45$–$60$ GeV, as measured by ATLAS [24]. Statistical uncertainties are shown as vertical lines and systematic uncertainties as filled boxes.

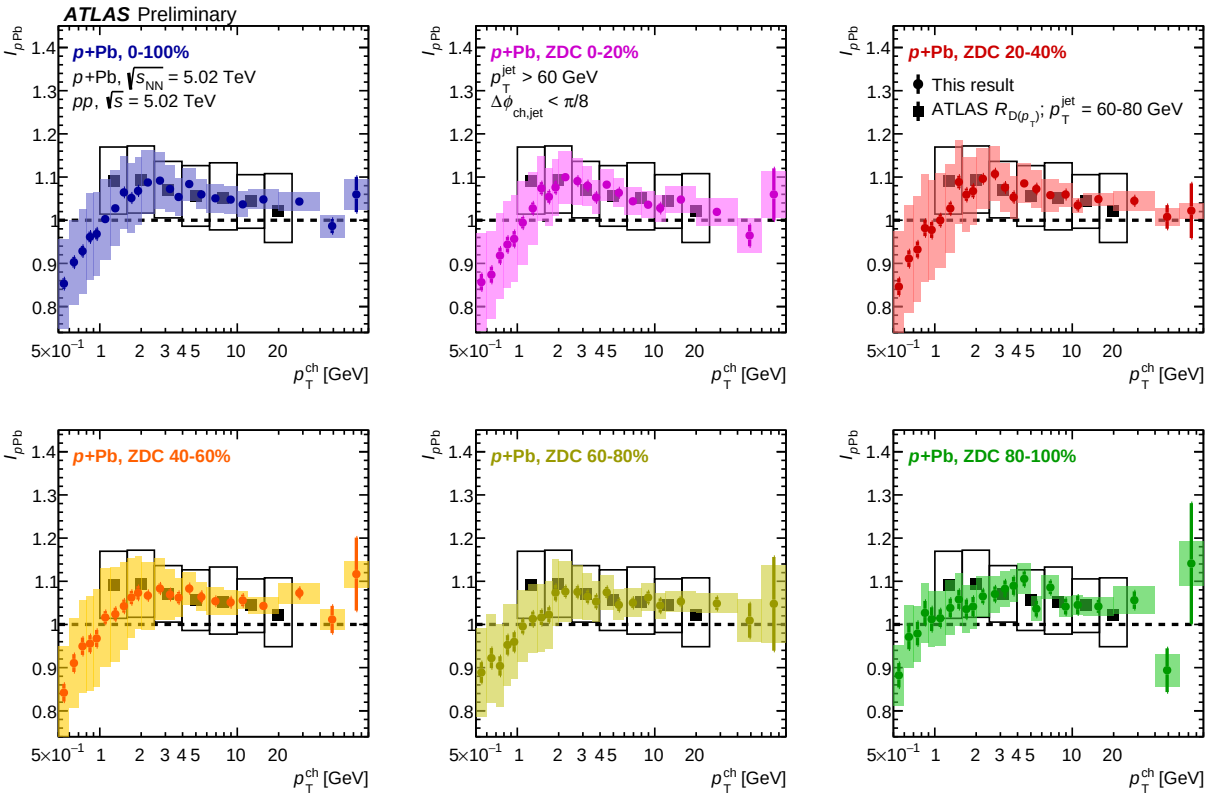


Figure 14: The ratio of per-jet charged particle yield in $p$+Pb and $pp$ collisions, $I_{p\mathrm{Pb}}$, for hadrons near a $p_{\mathrm{T}}^{\mathrm{jet}} > 60$ GeV jet ($\Delta\phi_{\mathrm{ch,jet}} < \pi/8$). Results are shown for different ZDC-selected $p$+Pb centralities in each panel. Also shown in square markers are ratios of the jet fragmentation function between centrality-inclusive $p$+Pb and $pp$ collisions for jets with $p_{\mathrm{T}}^{\mathrm{jet}} = 60$–$80$ GeV, as measured by ATLAS [24]. Statistical uncertainties are shown as vertical lines and systematic uncertainties as filled boxes.

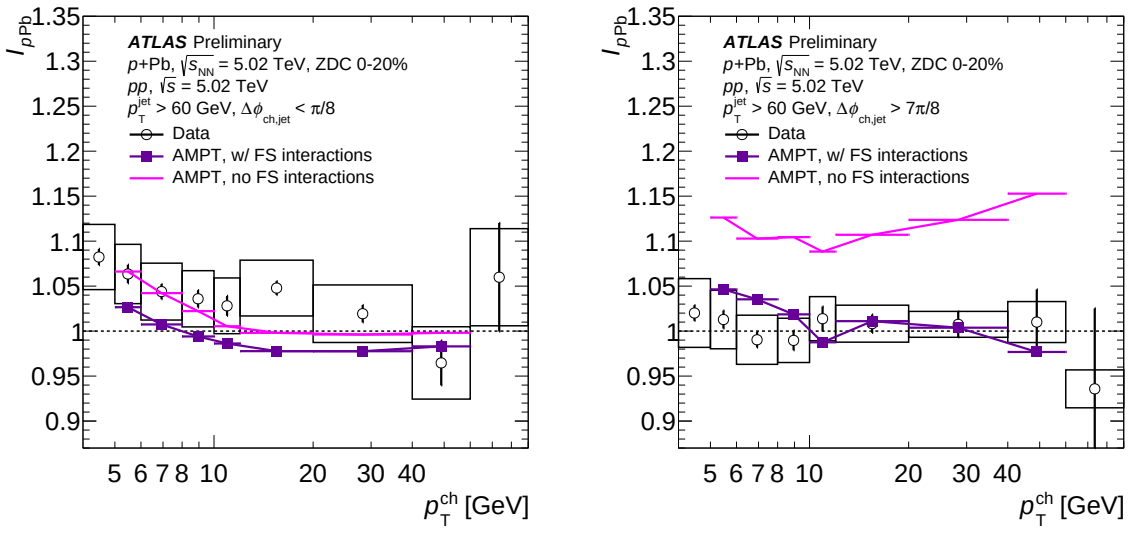


Figure 15: The ratio of per-jet charged particle yields $I_{p\mathrm{Pb}}$ on the near-side (left) and away-side (right) between $p$+Pb and $pp$ are plotted for the 0–20% $p$+Pb ZDC-selected centralities. Particles correlated with a jet above 60 GeV are shown. Also shown are calculations from the AMPT generator with and without final state (FS) interactions [61].

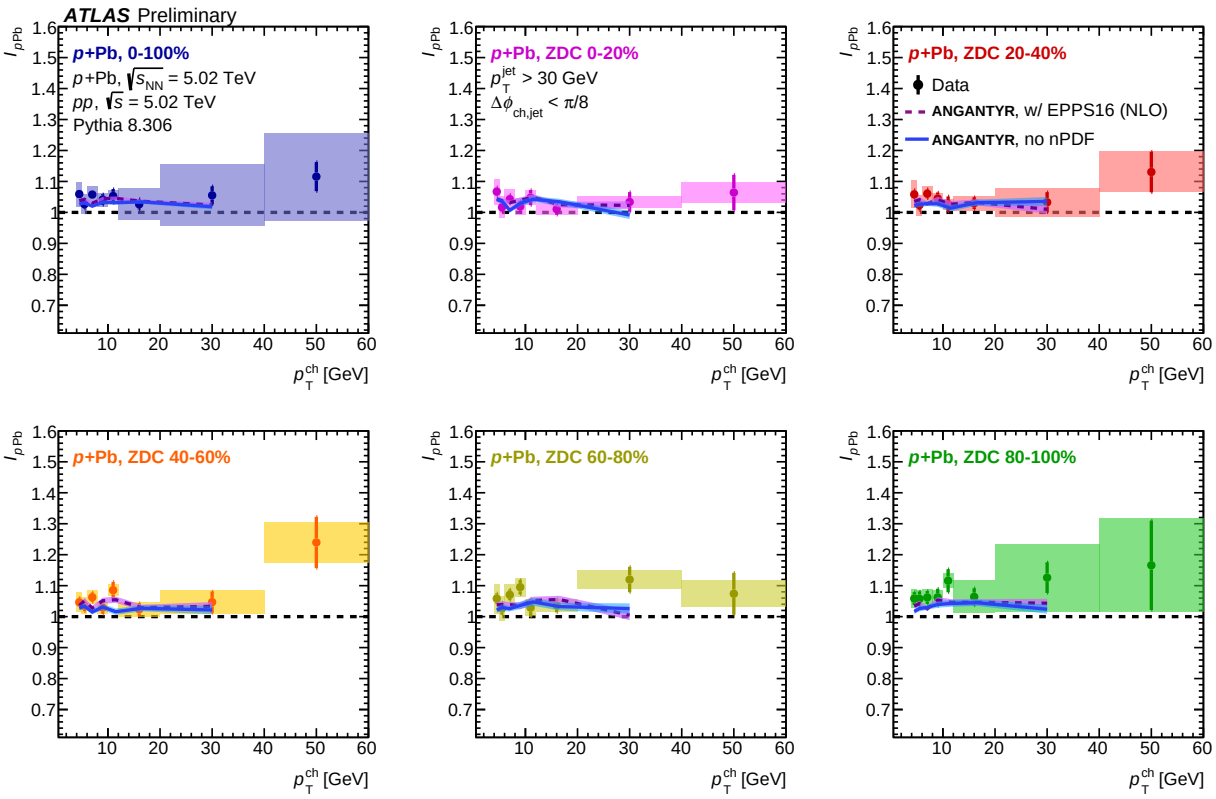


Figure 16: The ratio of per-jet charged particle yields in $p$+Pb and $pp$ collisions, $I_{p\mathrm{Pb}}$, for hadrons near a $p_{\mathrm{T}}^{\mathrm{jet}} > 30$ GeV jet ($\Delta\phi_{\mathrm{ch,jet}} < \pi/8$). Results are shown for different ZDC-selected $p$+Pb centralities in each panel. Also shown are calculations from the ANGANTYR generator [57] with and without nuclear modified parton distribution functions [58]. Statistical uncertainties are shown as vertical lines and systematic uncertainties as filled boxes.

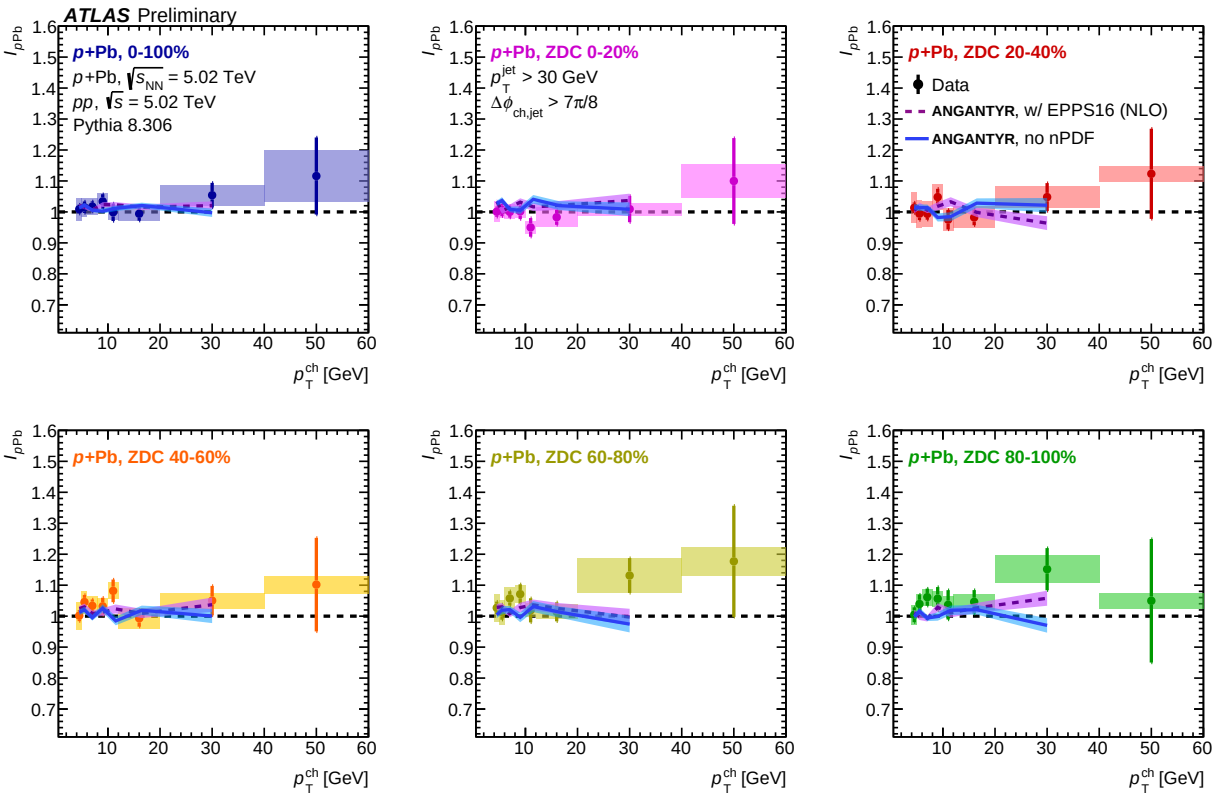


Figure 17: The ratio of per-jet charged particle yield in $p$+Pb and $pp$ collisions, $I_{p\mathrm{Pb}}$, for hadrons opposite to a $p_{\mathrm{T}}^{\mathrm{jet}} > 30$ GeV jet ($\Delta\phi_{\mathrm{ch,jet}} > 7\pi/8$). Results are shown for different ZDC-selected $p$+Pb centralities in each panel. Also shown are calculations from the ANGANTYR generator [57] with and without nuclear modified parton distribution functions [58]. Statistical uncertainties are shown as vertical lines and systematic uncertainties as filled boxes.

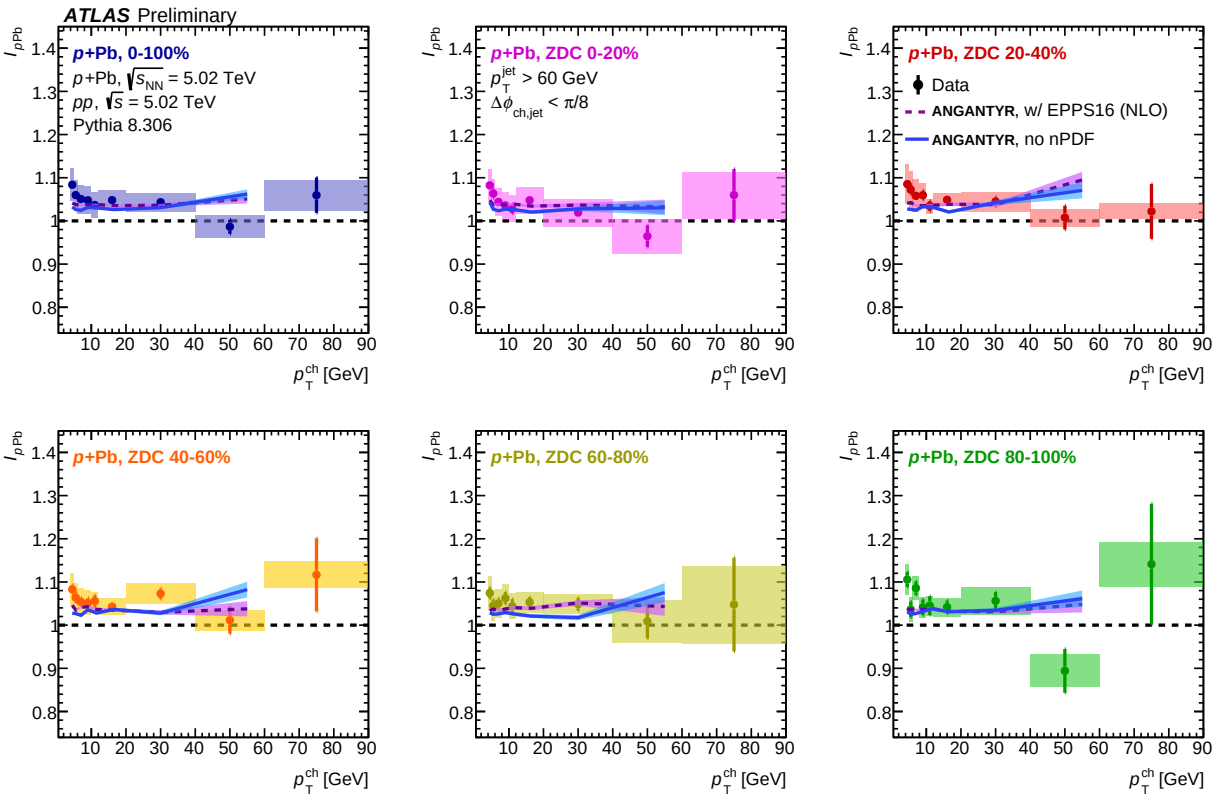


Figure 18: The ratio of per-jet charged particle yield in $p$+Pb and $pp$ collisions, $I_{p\mathrm{Pb}}$, for hadrons near a $p_{\mathrm{T}}^{\mathrm{jet}} > 60$ GeV jet ($\Delta\phi_{\mathrm{ch,jet}} < \pi/8$). Results are shown for different ZDC-selected $p$+Pb centralities in each panel. Also shown are calculations from the ANGANTYR generator [57] with and without nuclear modified parton distribution functions [58]. Statistical uncertainties are shown as vertical lines and systematic uncertainties as filled boxes.

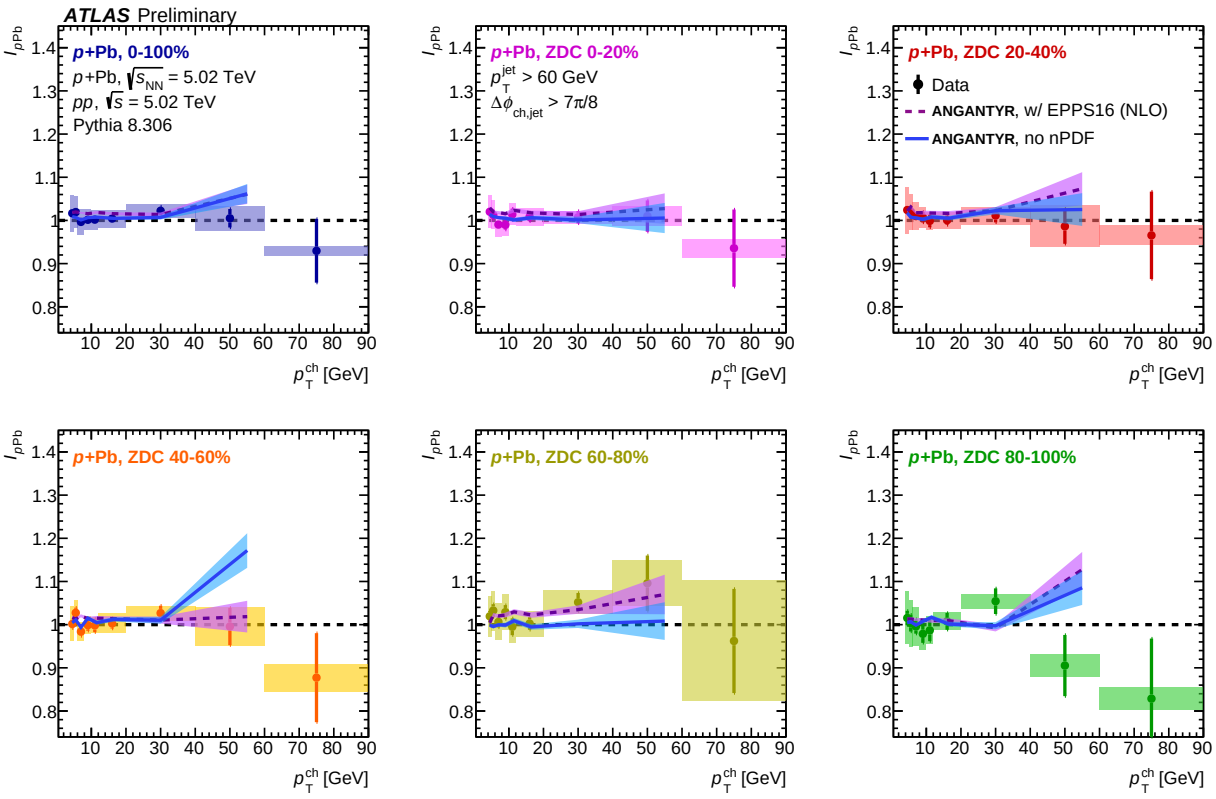


Figure 19: The ratio of per-jet charged particle yield in $p$+Pb and $pp$ collisions, $I_{p\mathrm{Pb}}$, for hadrons opposite to a $p_{\mathrm{T}}^{\mathrm{jet}} > 60$ GeV jet ($\Delta\phi_{\mathrm{ch,jet}} > 7\pi/8$). Results are shown for different ZDC-selected $p$+Pb centralities in each panel. Also shown are calculations from the ANGANTYR generator [57] with and without nuclear modified parton distribution functions [58]. Statistical uncertainties are shown as vertical lines and systematic uncertainties as filled boxes.

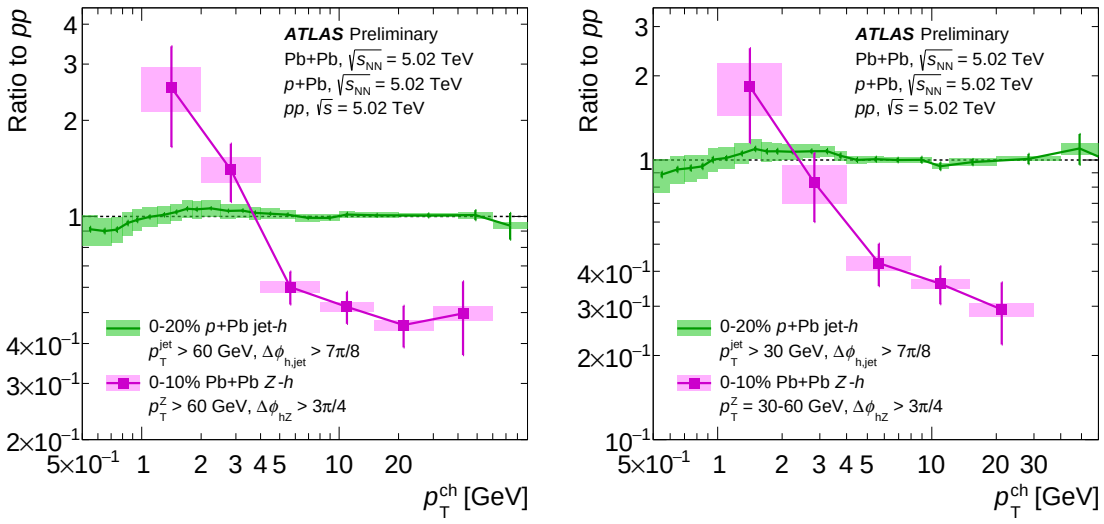


Figure 20: Comparison of the jet–hadron $I_{p\mathrm{Pb}}$ in 0–20% $p$+Pb collisions (green) with the $Z$–hadron $I_{\mathrm{AA}}$ in 0–10% Pb+Pb collisions (pink) from [62]. The left (right) panel shows the selections $p_{\mathrm{T}}^{\mathrm{jet}}$, $p_{\mathrm{T}}^{Z} > 30$ GeV ($> 60$ GeV). For both measurements, the statistical uncertainties are shown as vertical lines and systematic uncertainties as filled boxes.

## References


[1] U. Heinz and R. Snellings, *Collective flow and viscosity in relativistic heavy-ion collisions*, Ann. Rev. Nucl. Part. Sci. **63** (2013) 123, arXiv: 1301.2826 [nucl-th] (cit. on p. 2).

[2] L. Cunqueiro and A. M. Sickles, *Studying the QGP with Jets at the LHC and RHIC*, (2021), arXiv: 2110.14490 [nucl-ex] (cit. on p. 2).

[3] M. Connors, C. Nattrass, R. Reed and S. Salur, *Jet measurements in heavy ion physics*, Rev. Mod. Phys. **90** (2018) 025005, arXiv: 1705.01974 [nucl-ex] (cit. on p. 2).

[4] G.-Y. Qin and X.-N. Wang, *Jet quenching in high-energy heavy-ion collisions*, Int. J. Mod. Phys. E **24** (2015) 1530014, ed. by X.-N. Wang, arXiv: 1511.00790 [hep-ph] (cit. on p. 2).

[5] CMS Collaboration, *High precision measurements of Z boson production in PbPb collisions at* $\sqrt{s_{NN}} = 5.02$ *TeV*, (2021), arXiv: 2103.14089 [hep-ex] (cit. on p. 2).

[6] ATLAS Collaboration, *Z boson production in Pb+Pb collisions at* $\sqrt{s_{NN}} = 5.02$ *TeV measured by the ATLAS experiment*, Phys. Lett. B **802** (2020) 135262, arXiv: 1910.13396 [hep-ex] (cit. on p. 2).

[7] ALICE Collaboration, *Z-boson production in p-Pb collisions at* $\sqrt{s_{\mathrm{NN}}} = 8.16$ *TeV and Pb-Pb collisions at* $\sqrt{s_{\mathrm{NN}}} = 5.02$ *TeV*, JHEP **09** (2020) 076, arXiv: 2005.11126 [nucl-ex] (cit. on p. 2).

[8] ATLAS Collaboration, *Measurement of Z Boson Production in Pb-Pb Collisions at* $\sqrt{s_{NN}} = 2.76$ *TeV with the ATLAS Detector*, Phys. Rev. Lett. **110** (2013) 022301, arXiv: 1210.6486 [hep-ex] (cit. on p. 2).

[9] CMS Collaboration, *The production of isolated photons in PbPb and pp collisions at* $\sqrt{s_{NN}} = 5.02$ *TeV*, JHEP **07** (2020) 116, arXiv: 2003.12797 [hep-ex] (cit. on p. 2).

[10] J. L. Nagle and W. A. Zajc, *Small System Collectivity in Relativistic Hadronic and Nuclear Collisions*, Ann. Rev. Nucl. Part. Sci. **68** (2018) 211, arXiv: 1801.03477 [nucl-ex] (cit. on pp. 2, 7).

[11] P. Romatschke and U. Romatschke, *Relativistic Fluid Dynamics In and Out of Equilibrium*, Cambridge Monographs on Mathematical Physics, Cambridge University Press, 2019, ISBN: 978-1-108-48368-1, 978-1-108-75002-8, arXiv: 1712.05815 [nucl-th] (cit. on p. 2).

[12] A. Huss et al., *Discovering Partonic Rescattering in Light Nucleus Collisions*, Phys. Rev. Lett. **126** (2021) 192301, arXiv: 2007.13754 [hep-ph] (cit. on p. 2).

[13] A. Huss et al., *Predicting parton energy loss in small collision systems*, Phys. Rev. C **103** (2021) 054903, arXiv: 2007.13758 [hep-ph] (cit. on p. 2).

[14] J. Brewer, A. Huss, A. Mazeliauskas and W. van der Schee, *Ratios of jet and hadron spectra at LHC energies: measuring high-*$p_T$ *suppression without a pp reference*, (2021), arXiv: 2108.13434 [hep-ph] (cit. on p. 2).

[15] B. G. Zakharov, *Jet quenching from heavy to light ion collisions*, JHEP **09** (2021) 087, arXiv: 2105.09350 [hep-ph] (cit. on p. 2).

[16] X. Zhang and J. Liao,
*Jet Quenching and Its Azimuthal Anisotropy in AA and possibly High Multiplicity pA and dA Collisions*,
(2013), arXiv: 1311.5463 [nucl-th] (cit. on p. 2).

[17] K. Tywoniuk, *Is there jet quenching in pPb?*, Nucl. Phys. A **926** (2014) 85 (cit. on p. 2).

[18] C. Park, C. Shen, S. Jeon and C. Gale,
*Rapidity-dependent jet energy loss in small systems with finite-size effects and running coupling*,
Nucl. Part. Phys. Proc. **289-290** (2017) 289, arXiv: 1612.06754 [nucl-th] (cit. on p. 2).

[19] ATLAS Collaboration, *Centrality and rapidity dependence of inclusive jet production in* $\sqrt{s_{NN}} = 5.02$ *TeV proton-lead collisions with the ATLAS detector*, Phys. Lett. B **748** (2015) 392,
arXiv: 1412.4092 [hep-ex] (cit. on p. 2).

[20] ALICE Collaboration, *Measurement of charged jet production cross sections and nuclear modification in p-Pb collisions at* $\sqrt{s_{\mathrm{NN}}} = 5.02$ *TeV*, Phys. Lett. B **749** (2015) 68, arXiv: 1503.00681 [nucl-ex]
(cit. on p. 2).

[21] ATLAS Collaboration, *Measurement of flow harmonics with multi-particle cumulants in Pb+Pb collisions at* $\sqrt{s_{NN}} = 2.76$ *TeV with the ATLAS detector*, Eur. Phys. J. C **74** (2014) 3157,
arXiv: 1408.4342 [hep-ex] (cit. on p. 2).

[22] ALICE Collaboration, *Nuclear modification factor of light neutral-meson spectra up to high transverse momentum in p-Pb collisions at* $\sqrt{s_{NN}} = 8.16$ *TeV*, (2021), arXiv: 2104.03116 [nucl-ex]
(cit. on p. 2).

[23] CMS Collaboration,
*Charged-particle nuclear modification factors in PbPb and pPb collisions at* $\sqrt{s_{NN}} = 5.02$ *TeV*,
JHEP **04** (2017) 039, arXiv: 1611.01664 [hep-ex] (cit. on p. 2).

[24] ATLAS Collaboration, *Measurement of jet fragmentation in* 5.02 *TeV proton–lead and proton–proton collisions with the ATLAS detector*, Nucl. Phys. **A978** (2018) 65, arXiv: 1706.02859 [hep-ex]
(cit. on pp. 2, 5, 7, 17, 18).

[25] C. A. Salgado and J. P. Wessels, *Proton–Lead Collisions at the CERN LHC*,
Ann. Rev. Nucl. Part. Sci. **66** (2016) 449 (cit. on p. 2).

[26] ALICE Collaboration,
*Centrality dependence of particle production in p-Pb collisions at* $\sqrt{s_{\mathrm{NN}}}$*= 5.02 TeV*,
Phys. Rev. C **91** (2015) 064905, arXiv: 1412.6828 [nucl-ex] (cit. on pp. 2, 4).

[27] M. Gyulassy and X.-N. Wang, *HIJING 1.0: A Monte Carlo program for parton and particle production in high-energy hadronic and nuclear collisions*, Comput. Phys. Commun. **83** (1994) 307,
arXiv: nucl-th/9502021 (cit. on pp. 2, 4).

[28] PHENIX Collaboration, *Centrality categorization for* $R_{p(d)+A}$ *in high-energy collisions*,
Phys. Rev. C **90** (2014) 034902, arXiv: 1310.4793 [nucl-ex] (cit. on p. 2).

[29] PHENIX Collaboration, *Centrality-dependent modification of jet-production rates in deuteron-gold collisions at* $\sqrt{s_{NN}}$*=200 GeV*, Phys. Rev. Lett. **116** (2016) 122301, arXiv: 1509.04657 [nucl-ex]
(cit. on p. 2).

[30] M. Alvioli, B. A. Cole, L. Frankfurt, D. V. Perepelitsa and M. Strikman, *Evidence for x-dependent proton color fluctuations in pA collisions at the CERN Large Hadron Collider*, Phys. Rev. C **93** (2016) 011902, arXiv: 1409.7381 [hep-ph] (cit. on p. 2).

[31] M. Alvioli, L. Frankfurt, D. Perepelitsa and M. Strikman, *Global analysis of color fluctuation effects in proton– and deuteron–nucleus collisions at RHIC and the LHC*, Phys. Rev. D **98** (2018) 071502, arXiv: 1709.04993 [hep-ph] (cit. on p. 2).

[32] A. Bzdak, V. Skokov and S. Bathe, *Centrality dependence of high energy jets in p+Pb collisions at energies available at the CERN Large Hadron Collider*, Phys. Rev. C **93** (2016) 044901, arXiv: 1408.3156 [hep-ph] (cit. on p. 2).

[33] M. Kordell and A. Majumder, *Jets in d(p)-A Collisions: Color Transparency or Energy Conservation*, Phys. Rev. C **97** (2018) 054904, arXiv: 1601.02595 [nucl-th] (cit. on p. 2).

[34] D. V. Perepelitsa and P. A. Steinberg, *Calculation of centrality bias factors in p+A collisions based on a positive correlation of hard process yields with underlying event activity*, (2014), arXiv: 1412.0976 [nucl-ex] (cit. on p. 2).

[35] C. Loizides and A. Morsch, *Absence of jet quenching in peripheral nucleus–nucleus collisions*, Phys. Lett. B **773** (2017) 408, arXiv: 1705.08856 [nucl-ex] (cit. on p. 2).

[36] ALICE Collaboration, *Measurement of prompt $D^0$, $D^+$, $D^{*+}$, and $D_S^+$ production in p–Pb collisions at $\sqrt{s_{NN}} = 5.02$ TeV*, JHEP **12** (2019) 092, arXiv: 1906.03425 [nucl-ex] (cit. on p. 2).

[37] ALICE Collaboration, *Constraints on jet quenching in p-Pb collisions at $\sqrt{s_{NN}} = 5.02$ TeV measured by the event-activity dependence of semi-inclusive hadron-jet distributions*, Phys. Lett. B **783** (2018) 95, arXiv: 1712.05603 [nucl-ex] (cit. on p. 2).

[38] ATLAS Collaboration, *The ATLAS Experiment at the CERN Large Hadron Collider*, JINST **3** (2008) S08003 (cit. on p. 3).

[39] ATLAS Collaboration, *ATLAS Insertable B-Layer Technical Design Report*, ATLAS-TDR-19; CERN-LHCC-2010-013, 2010, URL: https://cds.cern.ch/record/1291633 (cit. on p. 3), Addendum: ATLAS-TDR-19-ADD-1; CERN-LHCC-2012-009, 2012, URL: https://cds.cern.ch/record/1451888.

[40] B. Abbott et al., *Production and integration of the ATLAS Insertable B-Layer*, JINST **13** (2018) T05008, arXiv: 1803.00844 [physics.ins-det] (cit. on p. 3).

[41] ATLAS Collaboration, *The ATLAS Collaboration Software and Firmware*, ATL-SOFT-PUB-2021-001, 2021, URL: https://cds.cern.ch/record/2767187 (cit. on pp. 3, 4).

[42] ATLAS Collaboration, *Performance of the ATLAS trigger system in 2015*, Eur. Phys. J. C **77** (2017) 317, arXiv: 1611.09661 [hep-ex] (cit. on p. 3).

[43] ATLAS Collaboration, *Vertex Reconstruction Performance of the ATLAS Detector at $\sqrt{s} = 13$ TeV*, ATL-PHYS-PUB-2015-026, 2015, URL: https://cds.cern.ch/record/2037717 (cit. on p. 3).

[44] M. Cacciari, G. P. Salam and G. Soyez, *The anti-$k_t$ jet clustering algorithm*, JHEP **04** (2008) 063, arXiv: 0802.1189 [hep-ph] (cit. on p. 4).

[45] M. Cacciari, G. P. Salam and G. Soyez, *FastJet User Manual*, Eur. Phys. J. C **72** (2012) 1896, arXiv: 1111.6097 [hep-ph] (cit. on p. 4).

[46] ATLAS Collaboration, *Dijet azimuthal correlations and conditional yields in pp and p + Pb collisions at $\sqrt{s_{NN}}$ = 5.02 TeV with the ATLAS detector*, Phys. Rev. C **100** (2019) 034903, arXiv: 1901.10440 [hep-ex] (cit. on p. 4).

[47] ATLAS Collaboration, *Charged-particle distributions in $\sqrt{s}$ = 13 TeV pp interactions measured with the ATLAS detector at the LHC*, Phys. Lett. B **758** (2016) 67, arXiv: 1602.01633 [hep-ex] (cit. on p. 4).

[48] T. Sjöstrand et al., *An introduction to PYTHIA 8.2*, Comput. Phys. Commun. **191** (2015) 159, arXiv: 1410.3012 [hep-ph] (cit. on pp. 4, 7).

[49] ATLAS Collaboration, *Measurement of the centrality dependence of the charged-particle pseudorapidity distribution in proton–lead collisions at $\sqrt{s_{NN}}$ = 5.02 TeV with the ATLAS detector*, Eur. Phys. J. C **76** (2016) 199, arXiv: 1508.00848 [hep-ex] (cit. on p. 4).

[50] G. D'Agostini, *A Multidimensional unfolding method based on Bayes' theorem*, Nucl. Instrum. Meth. A **362** (1995) 487 (cit. on p. 4).

[51] ATLAS Collaboration, *Jet energy scale measurements and their systematic uncertainties in proton–proton collisions at $\sqrt{s}$ = 13 TeV with the ATLAS detector*, Phys. Rev. D **96** (2017) 072002, arXiv: 1703.09665 [hep-ex] (cit. on p. 5).

[52] ATLAS Collaboration, *Jet energy scale and its uncertainty for jets reconstructed using the ATLAS heavy ion jet algorithm*, ATLAS-CONF-2015-016, 2015, URL: https://cds.cern.ch/record/2008677 (cit. on p. 5).

[53] ATLAS Collaboration, *Measurement of jet fragmentation in Pb+Pb and pp collisions at $\sqrt{s_{NN}}$ = 5.02 TeV with the ATLAS detector*, Phys. Rev. C **98** (2018) 024908, arXiv: 1805.05424 [hep-ex] (cit. on p. 5).

[54] ATLAS Collaboration, *Measurement of long-range multiparticle azimuthal correlations with the subevent cumulant method in pp and p+Pb collisions with the ATLAS detector at the CERN Large Hadron Collider*, Phys. Rev. C **97** (2018) 024904, arXiv: 1708.03559 [hep-ex] (cit. on p. 6).

[55] ATLAS Collaboration, *Transverse momentum, rapidity, and centrality dependence of inclusive charged-particle production in $\sqrt{s_{NN}}$ = 5.02 TeV p+Pb collisions measured by the ATLAS experiment*, Phys. Lett. B **763** (2016) 313, arXiv: 1605.06436 [hep-ex] (cit. on p. 6).

[56] J. W. Cronin et al., *Production of hadrons at large transverse momentum at 200, 300, and 400 GeV*, Phys. Rev. D **11** (11 1975) 3105, URL: https://link.aps.org/doi/10.1103/PhysRevD.11.3105 (cit. on p. 6).

[57] C. Bierlich, G. Gustafson, L. Lönnblad and H. Shah, *The Angantyr model for Heavy-Ion Collisions in PYTHIA8*, JHEP **10** (2018) 134, arXiv: 1806.10820 [hep-ph] (cit. on pp. 6, 7, 20–23).

[58] K. J. Eskola, P. Paakkinen, H. Paukkunen and C. A. Salgado, *EPPS16: Nuclear parton distributions with LHC data*, Eur. Phys. J. C **77** (2017) 163, arXiv: 1612.05741 [hep-ph] (cit. on pp. 6, 20–23).

[59] C. Bierlich, S. Chakraborty, G. Gustafson and L. Lönnblad,
*Setting the string shoving picture in a new frame*, JHEP **03** (2021) 270, arXiv: 2010.07595 [hep-ph] (cit. on p. 7).

[60] B. Muller, *Parton Energy Loss in Strongly Coupled AdS/CFT*,
Nucl. Phys. A **855** (2011) 74, ed. by I. Tserruya, A. Milov, D. d'Enterria, P. Jacobs and U. Wiedemann, arXiv: 1010.4258 [hep-ph] (cit. on p. 7).

[61] Z.-W. Lin, C. M. Ko, B.-A. Li, B. Zhang and S. Pal,
*A Multi-phase transport model for relativistic heavy ion collisions*, Phys. Rev. C **72** (2005) 064901, arXiv: nucl-th/0411110 (cit. on p. 19).

[62] ATLAS Collaboration, *Medium-Induced Modification of Z-Tagged Charged Particle Yields in Pb+Pb Collisions at* 5.02 *TeV with the ATLAS Detector*, Phys. Rev. Lett. **126** (2021) 072301, arXiv: 2008.09811 [hep-ex] (cit. on p. 24).